AD-A087 256 JOHNS HOPKINS UNIV LAUREL MD APPLIED PHYSICS LAB F/G 20/14
COMPARISON OF RADAR DERIVED RAIN ATTENUATION WITH THE COMSTAR B--ETC(U)
JUL 79 J GOLDHIRSH N00024-78-C-5384
UNCLASSIFIED APL/JHU-SIR79U-016 NL

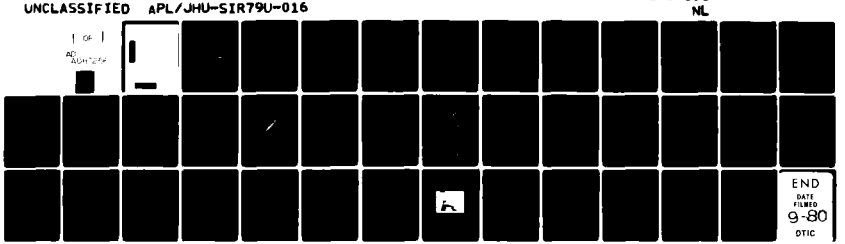

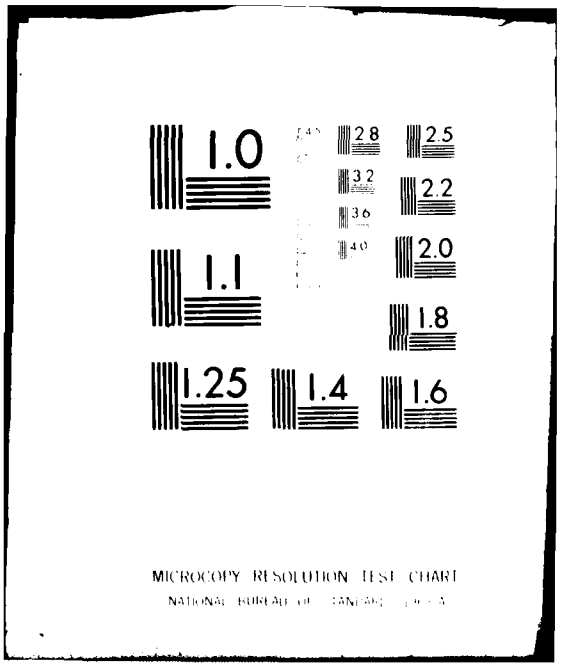
1.0
1.1
1.25
2.8
3.2
3.6
4.0
2.5
2.2
2.0
1.8
1.4
1.6
MICROCOPY RESOLUTION TEST CHART
NATIONAL BUREAU OF STANDARDS

(12) 37

(11) Jul 79

(14) APL/JHU-
SIR79U-Ø16
JULY 1979

COMPARISON OF RADAR DERIVED RAIN ATTENUATION WITH THE COMSTAR BEACON AT 28.56 GHz FOR SUMMER AND WINTER PERIODS

(10) ~~by~~ JULIUS/GOLDHIRSH

(15) N00024-78-C-5384

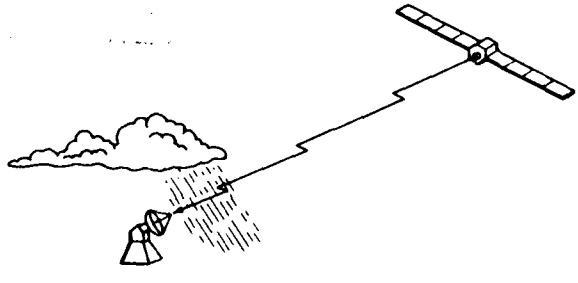

SPACE DEPARTMENT
THE JOHNS HOPKINS UNIVERSITY ■ APPLIED PHYSICS LABORATORY
Johns Hopkins Road, Laurel, Maryland 20810

Operating under Contract N00024-78-C-5384 with the Department of the Navy

TABLE OF CONTENTS

LIST OF FIGURES

List of Figures (continued)

THE JOHNS HOPKINS UNIVERSITY
APPLIED PHYSICS LABORATORY
LAUREL MARYLAND

COMPARISON OF RADAR DERIVED SLANT PATH RAIN ATTENUATION WITH THE COMSTAR BEACON FADES AT 28.56 GHz FOR SUMMER AND WINTER PERIODS

Abstract

A description of new results is given pertaining to an experiment whose aims are to test and improve the accuracy of radar derived slant path rain attenuation methods. These estimated results are compared with measured rain fade levels of the COMSTAR beacon signal at 28.56 GHz at Wallops Island, Virginia. The new data base corresponds to five rain days flanking the winter of 1978-79 during which 715 minutes of simultaneous radar and disdrometer data were obtained.

Agreement between estimated and measured individual rain fade events was found to be generally good. Agreement between corresponding conditional cumulative fade distributions was excellent.

As a basis for comparison with measured drop size spectra cases, the Marshall-Palmer distribution was injected into the radar program and found to give similarly good results for this data base. This result is consistent with the application of the Marshall-Palmer distribution for stratiform type rains as is generally the rain type for winter periods.

1.0 INTRODUCTION

Radar has represented a useful tool for the determination of conditional fade statistics from which single terminal and space diversity criteria have been established (1,2,3). Because radar has the intrinsic ability to characterize rain structure through beam scanning and establish enormous data bases over relatively short periods, considerable potential exists for utilizing it to establish absolute fade statistics and to extrapolate these statistics to other geographic locations (4). For these reasons a continuing program has been in effect since 1977 for testing and improving the accuracy of radar methods for estimating slant path attenuation.

Specifically, this report is an update of an experiment for testing and improving the accuracy of radar derived slant path attenuation of the 28.56 GHz COMSTAR beacon signal (5) using an electromechanical disdrometer located at Wallops Island, VA. In results previously published (6,7), it was demonstrated that radar derived attenuation events were in general good agreement with beacon measured levels and corresponding cumulative fade distributions obtained over simultaneous measurement periods gave very good agreement. The data base over which the above results were based consisted of five rain days in the summer of 1977 during which 304 minutes of simultaneous radar data were analyzed.

In this report we consider the results of an additional data base consisting of five rain days flanking the winter of 1978-79 during which 715 minutes of simultaneous radar and disdrometer data were obtained. Attenuation coefficient-reflectivity factor (k-Z) regression relationships were obtained from measured raindrop spectra and injected into the radar attenuation estimation technique. Individual attenuation events as well as cumulative conditional fade distributions are compared with corresponding beacon measured cases. Results pertaining to the overall data base for the Summer of 1977 and Fall-Winter 1978-79 are also analyzed.

2.0 EXPERIMENTAL ASPECTS

2.1 Configuration

Since the details of the on-going experiment at Wallops Island, VA, were described previously (6,7), only a short review is given here. The experimental configuration is depicted in Figure 1. Prior to 1 September 1978, the COMSTAR receiving antenna was looking at Satellite D2 and our elevation and azimuth angles were 41.6° and 210°, respectively. With the subsequent shutoff of D2, the antenna has been directed towards D3 (since 1 September 1978) with corresponding elevation and azimuth angles of 44.5° and 198.3°, respectively (see Table in Fig. 1).

The receiving antenna is fixed, has a beamwidth of 0.4°, and receives the 28.56 GHz signal continuously. During selected periods of rain, a high resolution S-band radar (0.4° beamwidth), located 30 m away, monitors the rain reflectivity at contiguous pulse volumes of 150 m resolution along the earth-satellite path. These reflectivities are recorded on IBM tape and are ultimately injected into a computer program which estimates the earth-satellite path attenuation with an integration time of 0.4 seconds. These radar estimated values are subsequently compared with the directly measured levels. During each rain storm, drop size distribution measurements are continuously made and these data are injected into the radar program for estimation of the path attenuation.

2.2 Revised Receiving System

During this past year we have modified our data acquisition system and made it more efficient. This modification has also given us the ability to monitor the receiver cross polarized isolation at 28.56 GHz.

The block diagram in Figure 2 depicts the revised configuration. The incoming co-polarization signal passes through a Faraday switch, is downconverted in the front end unit and the I.F. (1.05 GHz) passes to a phase locked loop receiver. The receiver output (0 to 5 volts) feeds into an A/D unit-switching

TYPE	SATELLITE LONG.	WI RECEIVER AZ	WI RECEIVER EL
D_1	128° W	244.8°	20.6°
D_2	95° W	210.0°	41.6°
D_3	87° W	198.3°	44.5°

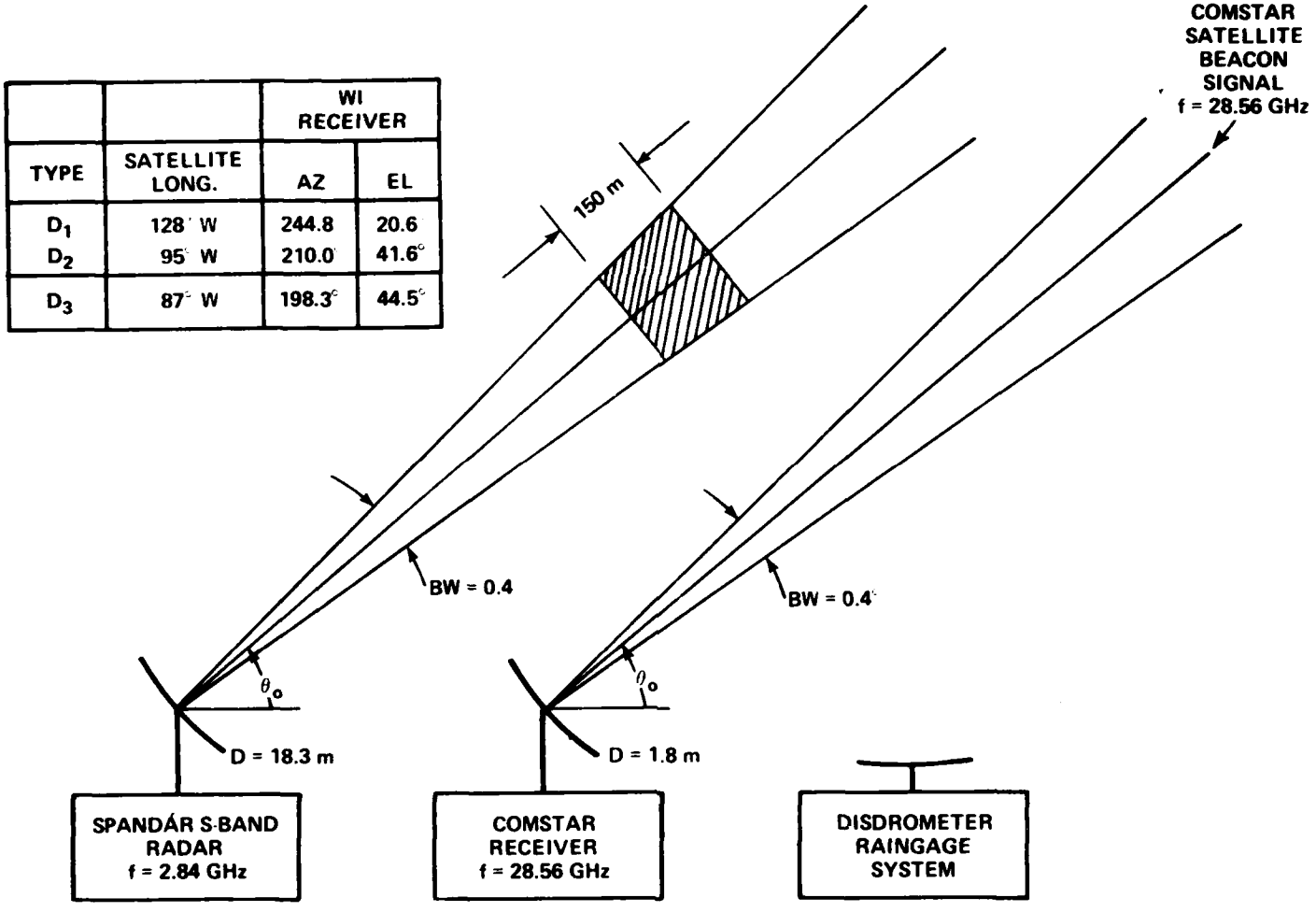

Figure 1. Experimental configuration at Wallops Island, Virginia.

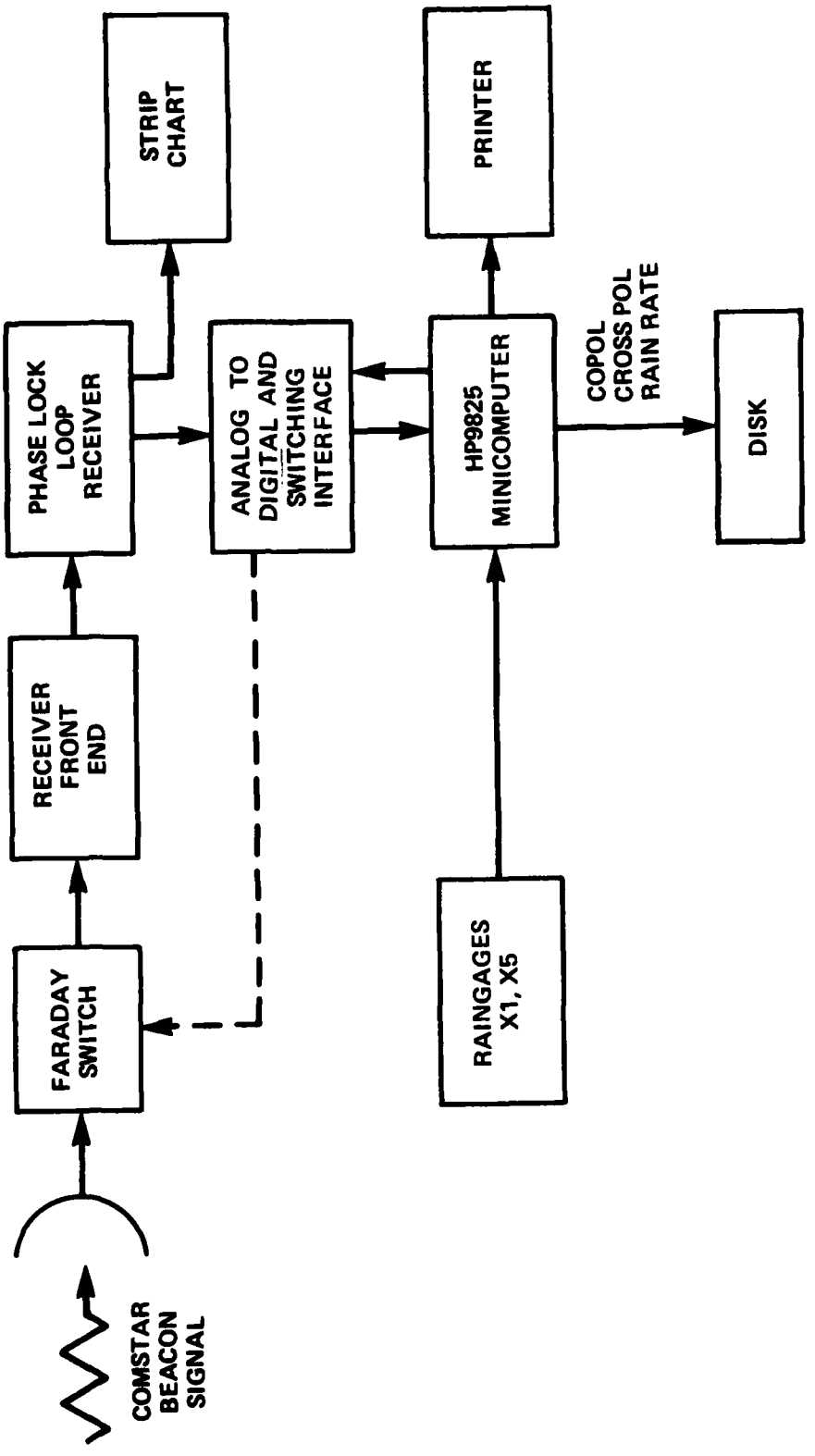

Figure 2. Simplified block diagram of system for monitoring co- and cross-polarization as well as simultaneous rain rates.

interface which injects the digitized receiver levels into an on-line HP 9825 minicomputer where it is sampled and recorded on magnetic disk. The switching interface also periodically transmits a current pulse to the Faraday switch which enables the cross polarized signal to pass into the receiver with negligible insertion loss while isolating the co-polarized signal (isolation being 26-27 dB). Both co and cross polarized signal levels are recorded on magnetic disk once per two seconds.

In addition, rain rates from two tipping bucket raingages, one with an enlarged funnel for improving the time resolution of smaller rain rates, is recorded simultaneously on the magnetic disk. Time is also recorded periodically from an internal clock in the minicomputer. Data is recorded continuously for a period of 65 hours on each disk side. System calibrations are performed by injecting 28.56 GHz signal levels through the front end and these are recorded on a disk which is later recalled for reduction of the data.

3.0 ANALYTIC ASPECTS

3.1 Review of Radar Estimation Formulation

We review here the mechanism by which attenuation is estimated using radar and disdrometer data.

The radar power recorded in each of the adjacent range bins is converted into reflectivity factor levels, $Z(mm^6/m^3)$ and these are injected in the formula for path attenuation given by,

$$A_R(t) = \sum_{i=1}^{N} k_i \, \Delta r \qquad (dB) \tag{3.1}$$

and

$$k_i = aZ_i^{\,b} \qquad (dB/km) \tag{3.2}$$

and where

$A_R(t)$ = the radar estimated attenuation at time, t (dB)
k_i = the attenuation coefficient pertaining to i^{th} range bin (dB/km)
Z_i = the reflectivity factor at i^{th} range bin (mm^6/m^3)
Δr = range resolution interval (150 m)
N = number of range bins used in summation (see text)

The limit, N, in (3.1) is obtained in the following way. Through the observation of photographs of RHI's taken at 1/2 to 1 hour intervals, it is noted as to whether the rains are either convective or non-convective; the latter showing a bright band and the former showing cellular activity rising to elevations above the zero degree isotherm height. The summation is taken up to the melting layer when a bright band appears since the dominant presence of ice above this height causes negligible attenuation. On the other hand, the summation is taken along the entire path when the rain is convective; implying the dominant presence of water above the zero degree isotherm height. This procedure has been found to give good results both in previous works (6,7,8) as well as in the present experiment. A further elaboration is given in Section 7.

The values of a and b were arrived at by sampling continuous 30 second drop size distributions (hereafter referred to as DSD) with the APL disdrometer during each rain period and calculating

$$k = \int_{D_{min}}^{D_{max}} N(D) C_{ext}(D)\, dD \qquad (dB/km) \tag{3.3}$$

$$Z = \int_{D_{min}}^{D_{max}} N(D) D^6 dD \qquad (mm^6/m^3) \tag{3.4}$$

where

k = theoretical attenuation coefficient (dB/km)
$N(D)dD$ = number of drops per unit volume between drop sizes D and D+dD (DSD)
$C_{ext}(D)$ = extinction factor (dB/km) x cm^3
Z = theoretical reflectivity factor (mm^6/m^3)
D_{min}, D_{max} = the minimum and maximum diameters measured, respectively.

Best fit values of a and b were generated for each rain period; the rain period representing a continuous rain event for the day in question. The extinction factors for 28.56 GHz, $C_{ext}(D)$, were arrived at by interpolating the results of Medhurst (9).

4.0 COMPARISON OF k-Z REGRESSION RELATIONSHIPS

In this section we compare the k-Z regression relationship from the measured rain drop spectra for the individual rain days during which simultaneous radar data were acquired. In Table 1 are listed the best fit values of a and b for the individual rain days as well as the % rms deviation of k from these best fit curves for the summer of 1977 and winter 1978-79. We note the average % rms deviations for the winter of 78-79 and summer of 1977 to be 28.5% and 21.6%; where the weighting factor is the number of disdrometer derived pairs of k-Z values (last column of Table 1).

The rows labeled "overall" give the columnar values when all the data are considered together for the indicated season periods. It is interesting to note that "overall" DSD derived k-Z regression relationships for the individual seasons and for the combined seasons are similar to the M-P case. For example, the combined overall data base (1977, 1978-79) in the reflectivity factor interval 10^3 to 10^5 (mm^6/m^3) have k values which are within 10% of one another.

In Figure 3 are plotted the individual k-Z regression curves for the winter period 1978-79. If the $\pm$ % rms of the

Table 1

COMPARISON BEST FIT PARAMETERS FOR $k = aZ^b$ FROM MEASURED RAINDROP SPECTRA

Date	a	b	% rms	No of Pts
Winter 1978-79				
November 27 (1978)	7.67×10^{-3}	0.598	32.8	120
January 2 (1979)	5.065×10^{-4}	0.892	34.7	116
January 24	5.29×10^{-3}	0.683	26.8	101
March 6	2.025×10^{-3}	0.806	29.2	181
April 4	3.49×10^{-3}	0.724	13.0	78
OVERALL 1978,1979 Weighted Avg	4.56×10^{-3}	0.687	36.1 28.5	596
Summer 1977				
June 6 (1977)	1.17×10^{-3}	0.825	24.6	123
June 9	7.36×10^{-3}	0.617	22.7	180
August 24	1.23×10^{-2}	0.492	15.8	102
August 25	1.45×10^{-3}	0.806	25.7	107
September 14	3.47×10^{-3}	0.733	14.3	53
OVERALL 1977 Weighted Avg	1.87×10^{-3}	0.775	30.0 21.6	565
OVERALL 1977,1978-79 Weighted Avg	2.74×10^{-3}	0.738	32.7 25.1	1161
M-P	2.01×10^{-3}	0.773		

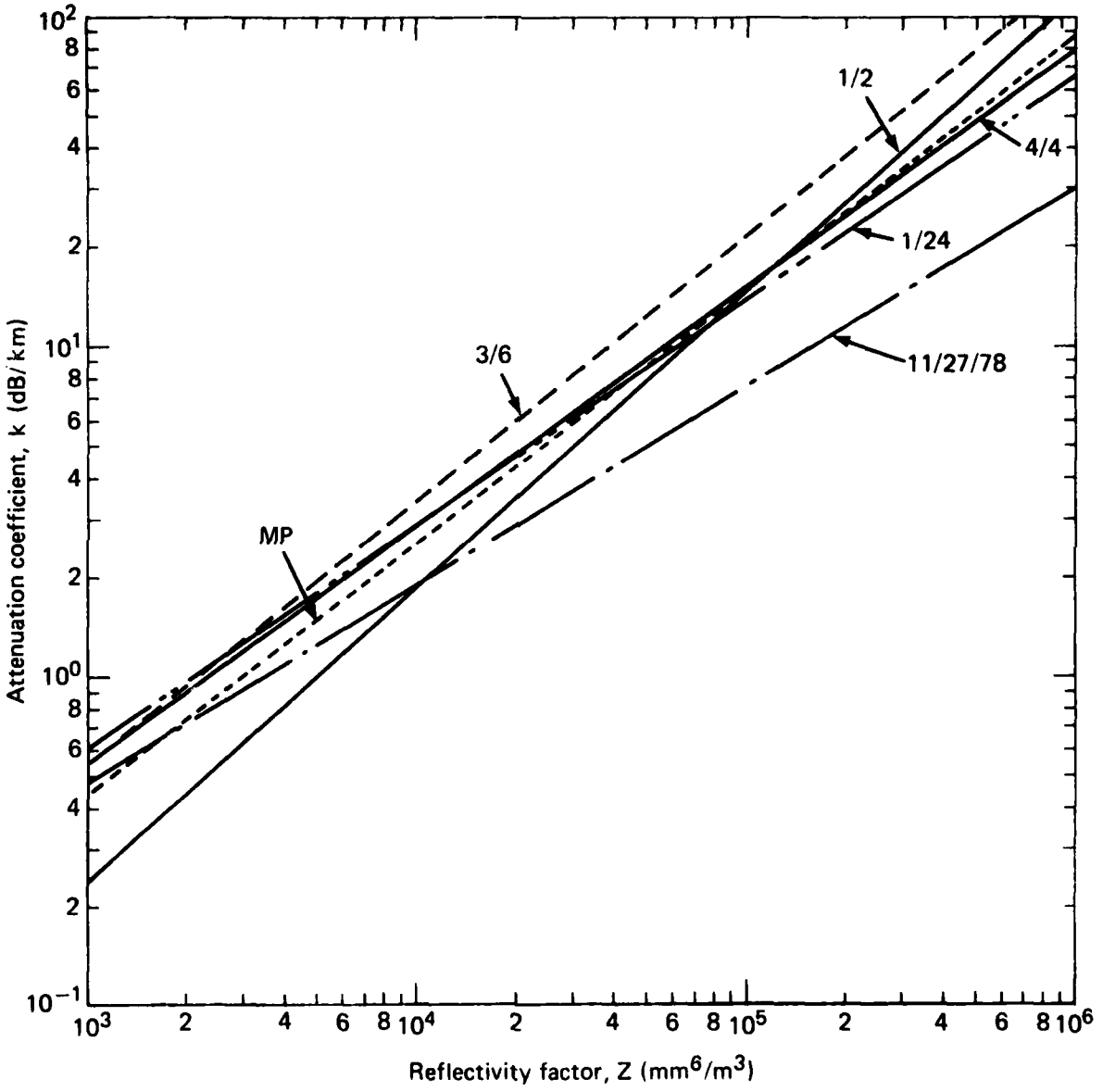

Figure 3. Comparison of derived $k = aZ^b$ best fit regression curves from disdrometer data for individual rain days.

individual days were included, all the curves would either overlap or be close to the M-P curve.

It is interesting to note that the % rms deviations during the summer of 1977 were, in general, smaller than those measured during the winter of 1978-79. This might be attributed to the nature of the summer rains (convective) as compared with the winter rains (stratiform).

It may also be noted that regression relationships arrived at for the rain days during the winter of 1978-79 were closer to the M-P case than those obtained during the summer of 1977. Again, this may be attributable to the fact that the M-P distribution is more applicable for stratiform rains than for convective types.

As an illustration of the proximity of the overall DSD and M-P data bases, we show plotted in Figure 4 a scatter plot diagram depicting the overall winter 1978-79 data base of disdrometer derived results. The ordinate represents the Log_{10} of the reflectivity factor, Z (mm^6/m^3). Each point represents an integrated drop size distribution of 2000 drops from which the values of k and Z were calculated using Eqs. (3.3) and (3.4). The solid curve represents the best fit $k = aZ^b$ regression curve and the dashed curve represents the M-P case. The M-P case is within $\pm$ 36% rms of the DSD curve over the reflectivity factor range 350 to 10^6 mm^6/m^3.

4.1 Comparison of Cumulative Distributions Derived from the Disdrometer and Raingage

In Figure 5 we show plotted two cumulative distributions of rain rates extracted from a tipping bucket raingage and a disdrometer, respectively. These results pertain to the simultaneous time periods (radar versus beacon) for the five rain days (727 minutes) during the fall-winter of 1978-79. We note that disdrometer distribution shows an approximate 9% rms deviation relative to the raingage curve for probability values down to

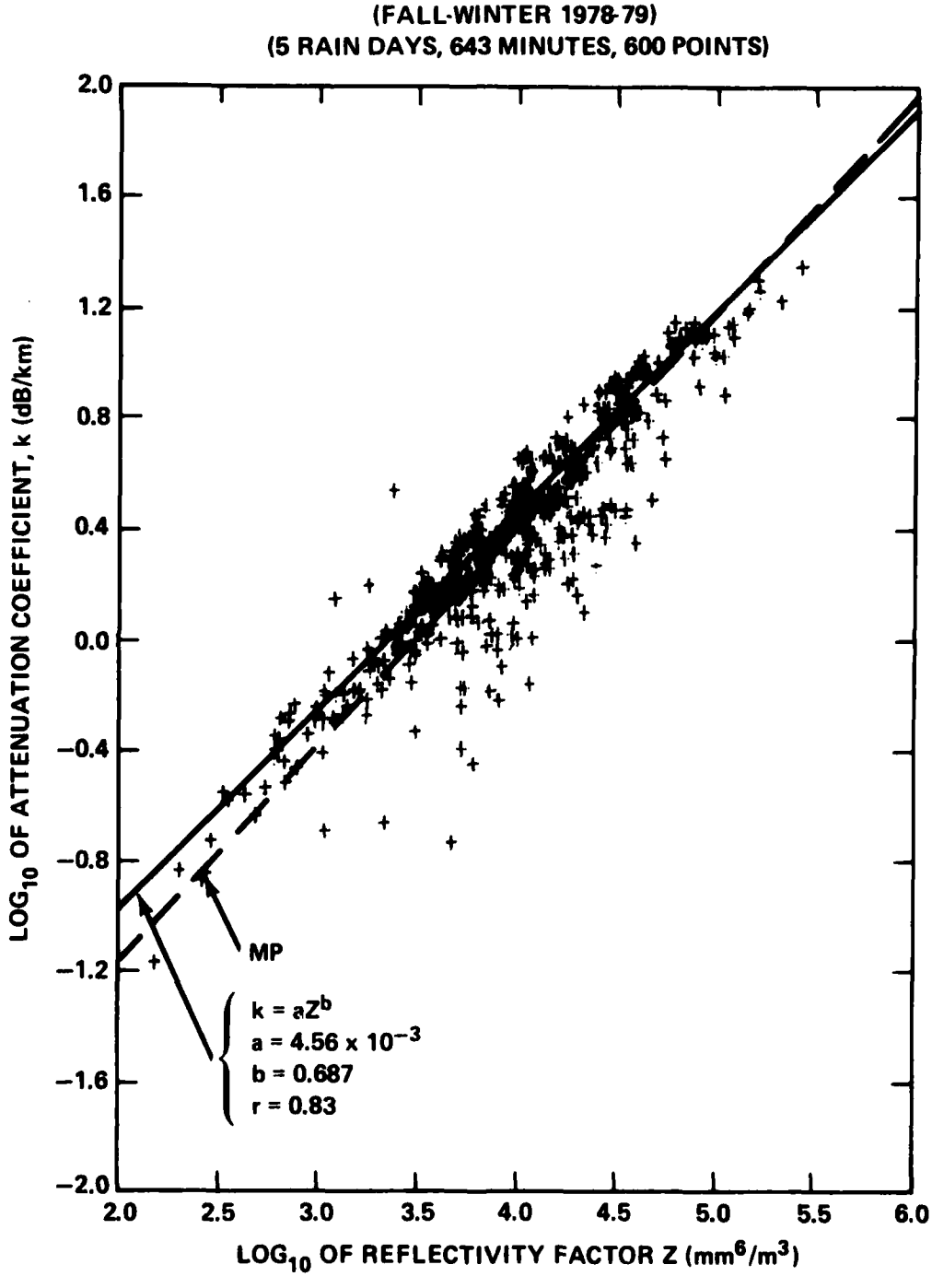

Figure 4. Scatter diagram of Log_{10} k vs Log_{10} Z for total of five rain days during the fall-winter period of 1978-79. Solid and dashed lines are best fit regression and Marshall-Palmer cases, respectively.

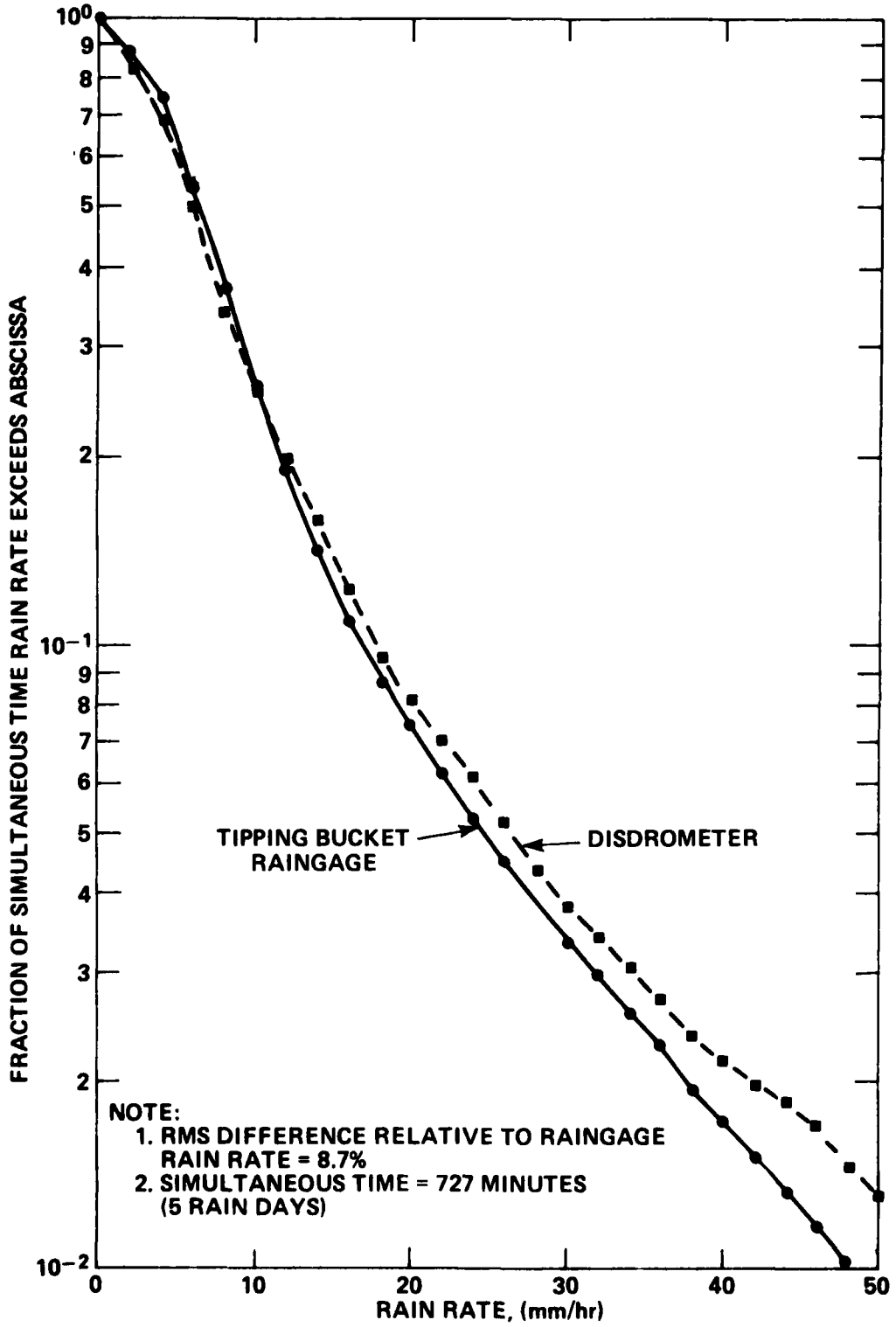

Figure 5. Comparison of conditional cumulative rain rate distributions derived from a raingage and disdrometer, respectively, for the fall-winter period 1978-79. The data base covers the simultaneous radar and beacon measurement periods (five rain days, 727 minutes).

.015. At smaller probabilities the data appears noisy. The close proximity of these two curves represents a partial check on the validity of the disdrometer data and a measure of the relative accuracy of the rain rate measurements.

5.0 COMPARISON OF MEASURED AND ESTIMATED ATTENUATION EVENTS

In this section we show comparisons between measured and estimated fade events for each of the five rain days (Figures 6-10). The ordinate in these figures represents the attenuation relative to the free space value and the abscissa is the time in GMT; local time being five hours less. The fixed level beacon fades on days 002 (Fig. 7), 024 (Fig. 8), and 094 (Fig. 10) represent the loss of phase lock condition which is approximately 30 dB. We note that in all of these cases the radar was capable of estimating fades well in excess of 30 dB. Furthermore, we note that the beacon case shows a lag in the re-acquisition of phase lock in comparison to the radar estimated cases. This behavior is probably due to the receiver characteristics. First of all, re-acquisition does not occur until the receiver fade levels reach approximately 25 dB. No such constraint exists for the radar attenuation estimation case. Secondly, when loss of lock exists, the receiver reverts to a frequency search mode and it may take one or more minutes before the receiver is tuned to the proper frequency and re-acquisition occurs. With this in mind, the estimated and measured fades for days 331 (Fig. 6), 002 (Fig. 7), and 024 (Fig. 8) show good agreement, day 065 (Fig. 9) fair agreement, and 094 (Fig. 10) fair to poor agreement. In weighting the overall results in terms of observation time, the combined comparisons may be considered to be generally good.

As a basis for comparison, the fixed Marshall-Palmer (10) k-Z regression relationship was also injected into the radar attenuation estimation program and similar overall agreement (not shown in Figures) was achieved when compared to the beacon levels. This agreement may be attributed to the fact that the measured k-Z expressions were either similar or had margin of uncertainties which for the most part overlapped with the fixed M-P case.

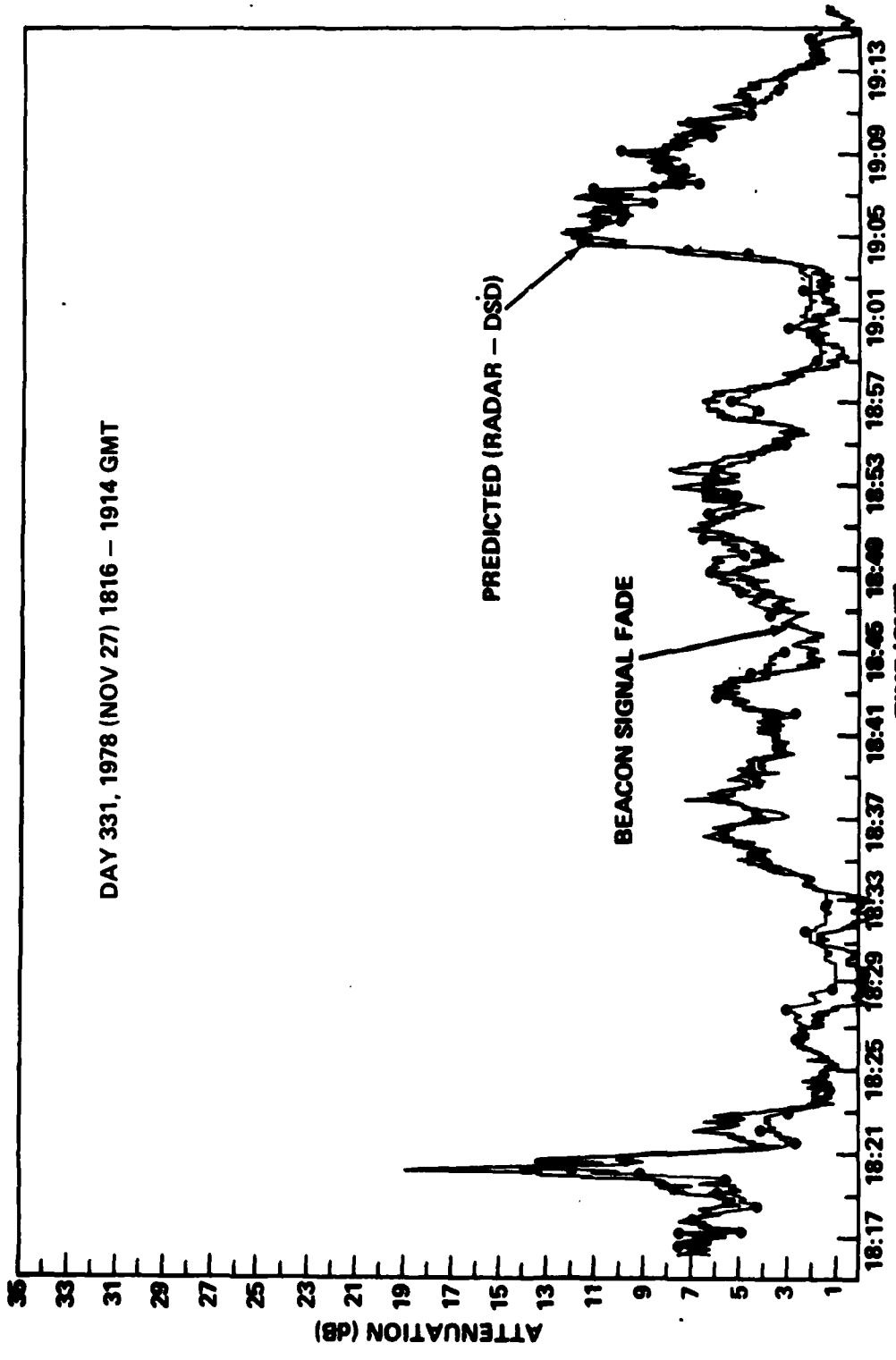

Figure 6. Comparison of radar derived and measured fade events for November 27, 1978 (Day 331); 1816 to 1914 GMT.

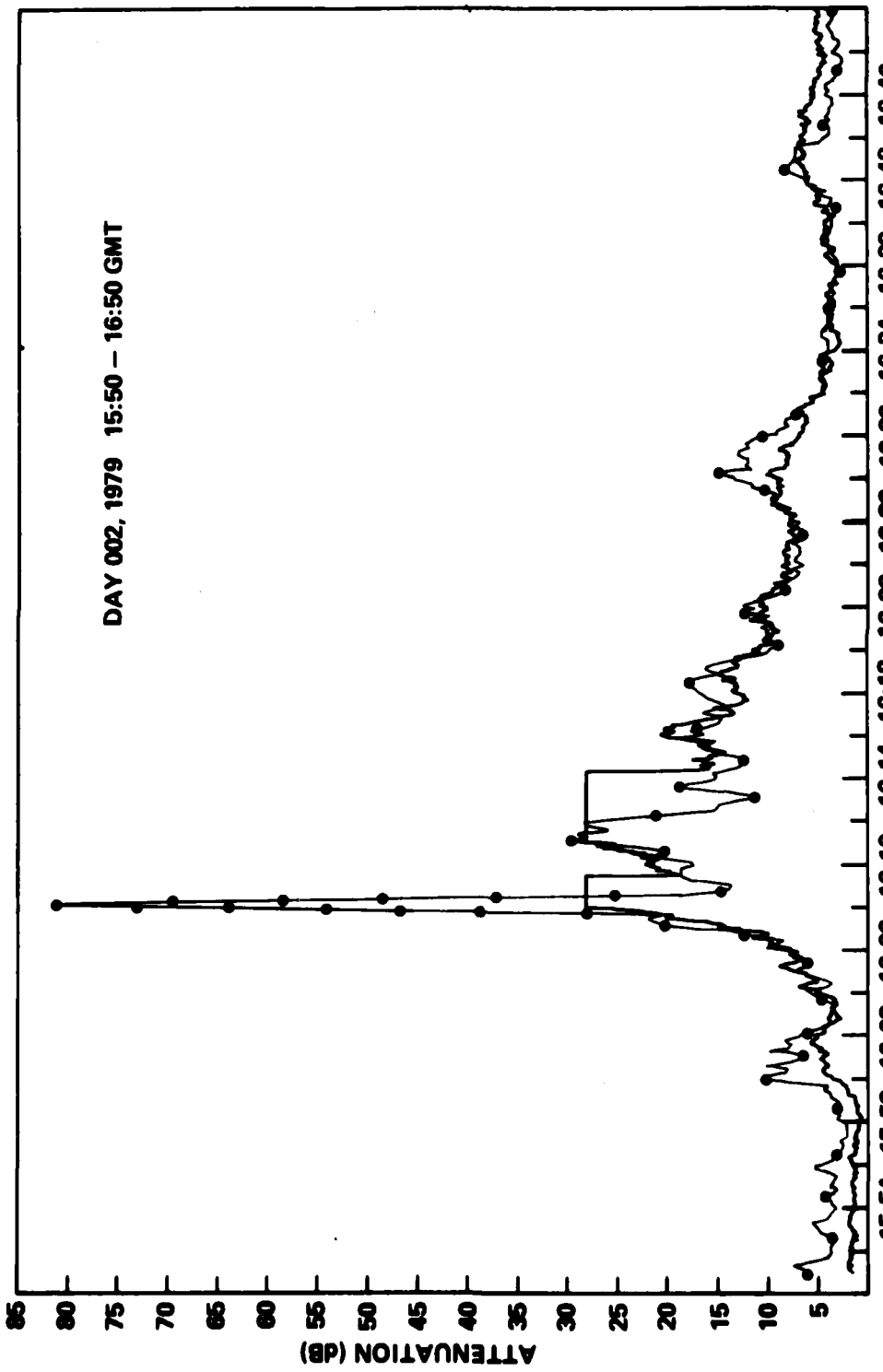

Figure 7. Comparison of radar derived and measured fade events for January 2, 1979 (Day 002); 1550 to 1650 GMT.

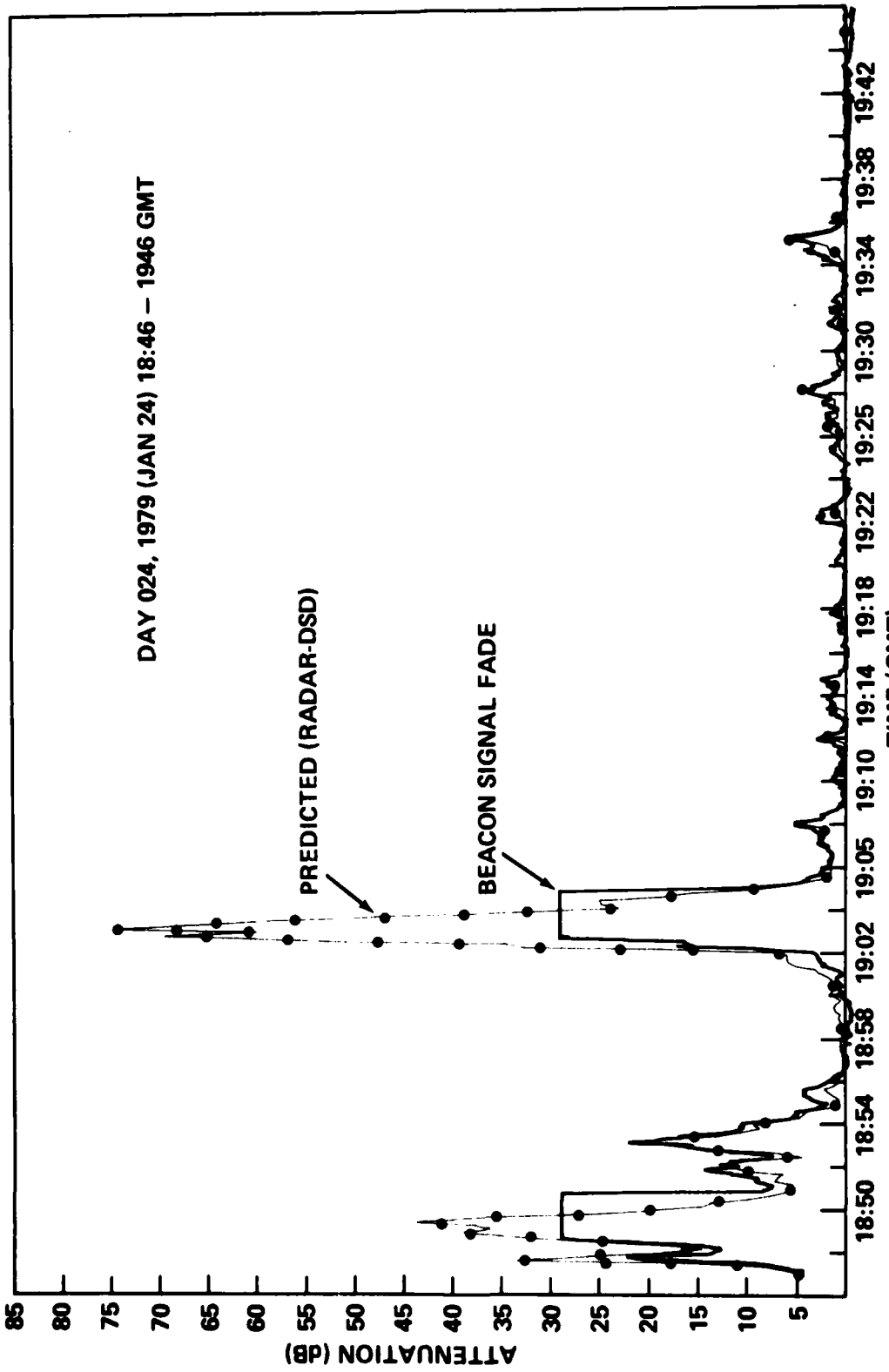

Figure 8. Comparison of radar derived and measured fade events for January 24, 1979 (Day 024); 1846 to 1946 GMT.

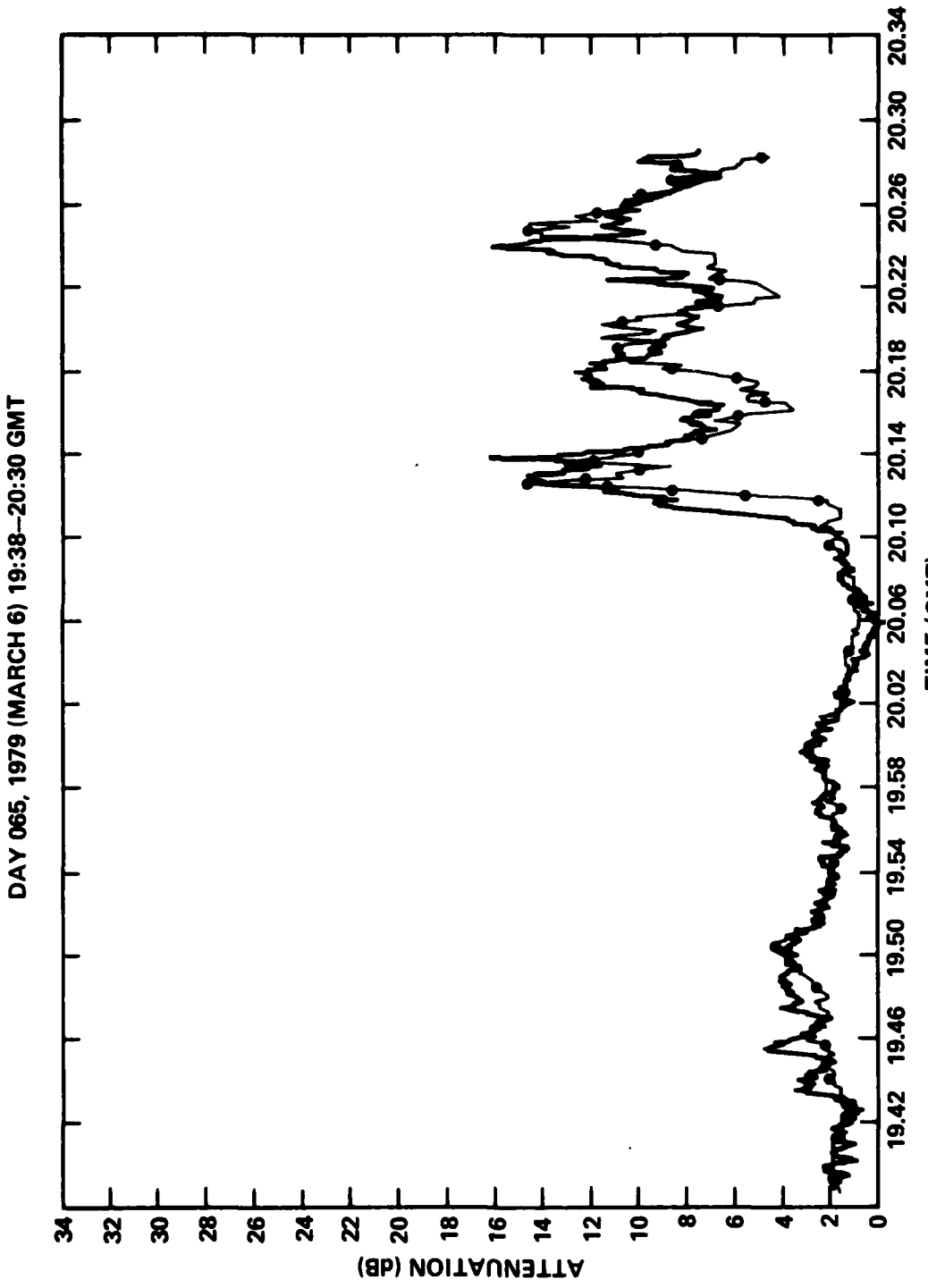

Figure 9. Comparison of radar derived and measured fade events for March 6, 1979 (Day 065); 1438 to 2030 GMT.

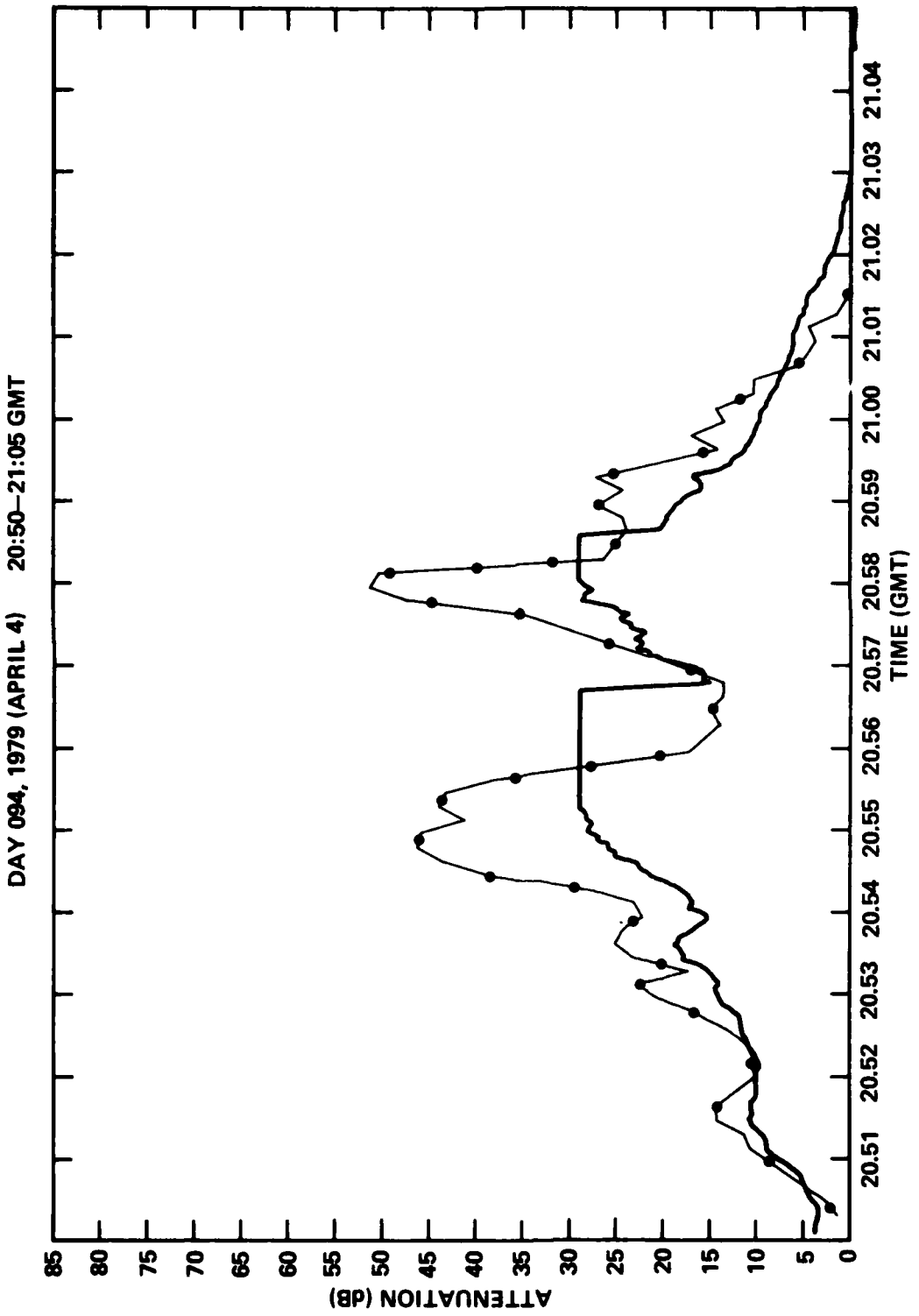

Figure 10. Comparison of radar derived and measured fade events for April 4, 1979 (Day 094); 2050 to 2105 GMT.

6.0 COMPARISON OF MEASURED AND ESTIMATED CUMULATIVE CONDITIONAL FADE DISTRIBUTIONS

In this Section we compare the cumulative conditional fade statistics associated with the measured and radar DSD and M-P estimated cases. These comparisons are given in Figures 11 through 13 and represent the summer of 1977 (a review), fall-winter 1978-79, and the combined simultaneous data base, respectively. In Table 2 the comparisons are expressed numerically in terms of the rms dB deviation, average dB deviation, and the average probability ratio. The rms and average dB deviations were obtained from the magnitudes of the dB differences between the measured and estimated curves for a series of fixed probabilities down to 25 dB. The average probability ratios were obtained by averaging the ratio of the larger probability to the smaller one for a series of fixed fade depths.

In all cases (Figs. 11-13), the DSD-radar case compares very well with the beacon measured one giving an rms deviation of approximately 1 dB. The proximity of the MP and DSD cases for the fall-winter 1978-79 (Fig. 12) may again be attributed to the fact that when the $\pm$ rms levels (Table 1) are included in the k-Z regression relationships of Figure 3, the error curves overlap or are close to the M-P curve over most of the important Z range. Hence the DSD and M-P, in general, give similar margins of errors relative to the beacon measured cases. We note that the results for the summer of 1977 show the M-P-radar estimated curve (Fig. 11) compares poorly with the beacon measured case (rms = 5.6 dB). For this data base, the measured k-Z regression relationships for some days were distinctly different than the M-P relationship.

7.0 MELTING LAYER EFFECTS

The rain flanking the fall-winter 1978-79 were predominantly widespread as is characteristic during such seasons. The radar returns from the zero degree isotherm region were, in general, very pronounced due to enhanced scattering from the

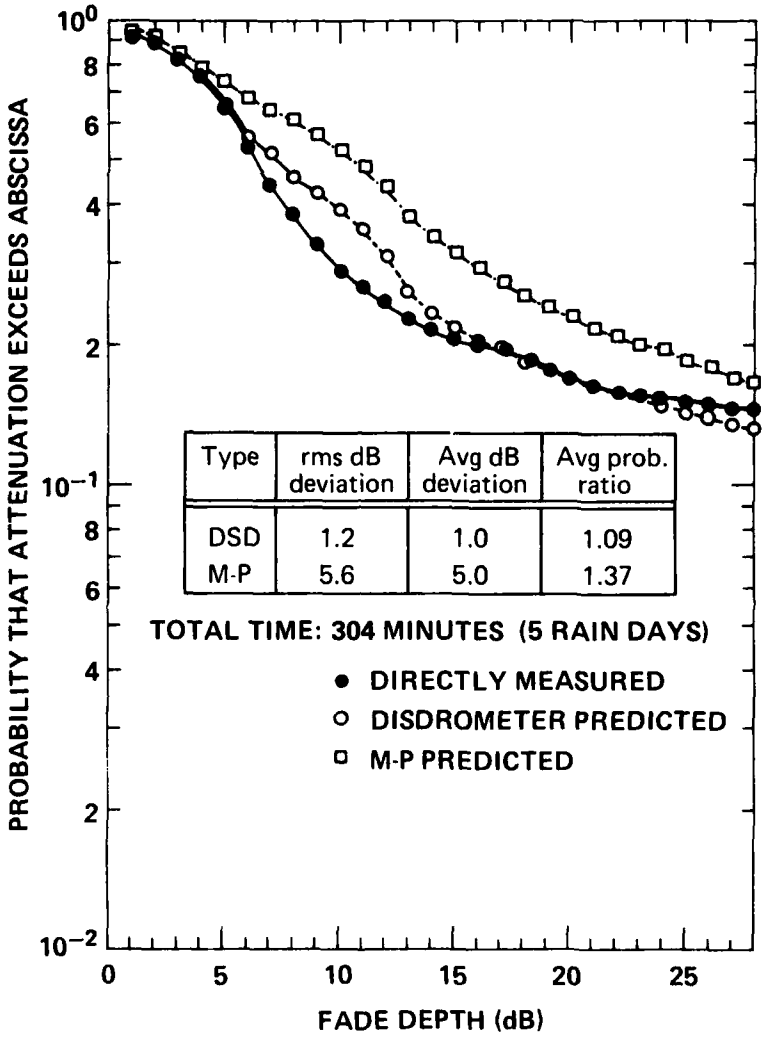

Figure 11. Comparison of directly measured and radar derived conditional cumulative distributions for summer of 1977 (five rain days, 304 minutes of simultaneous data).

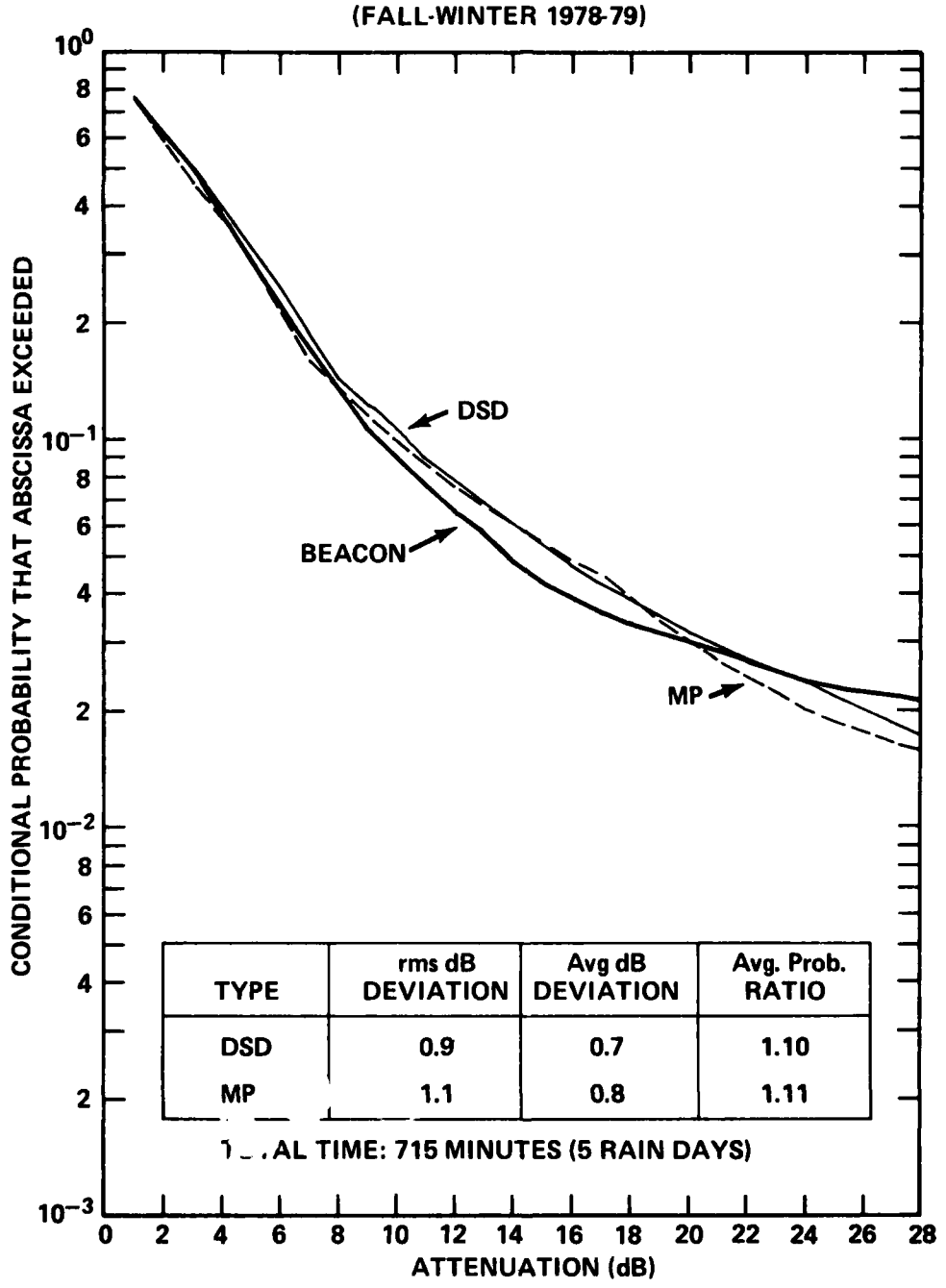

Figure 12. Comparison of directly measured and radar derived conditional cumulative distributions for rain days about the fall-winter 1978-79 period (five rain days, 715 minutes of simultaneous data).

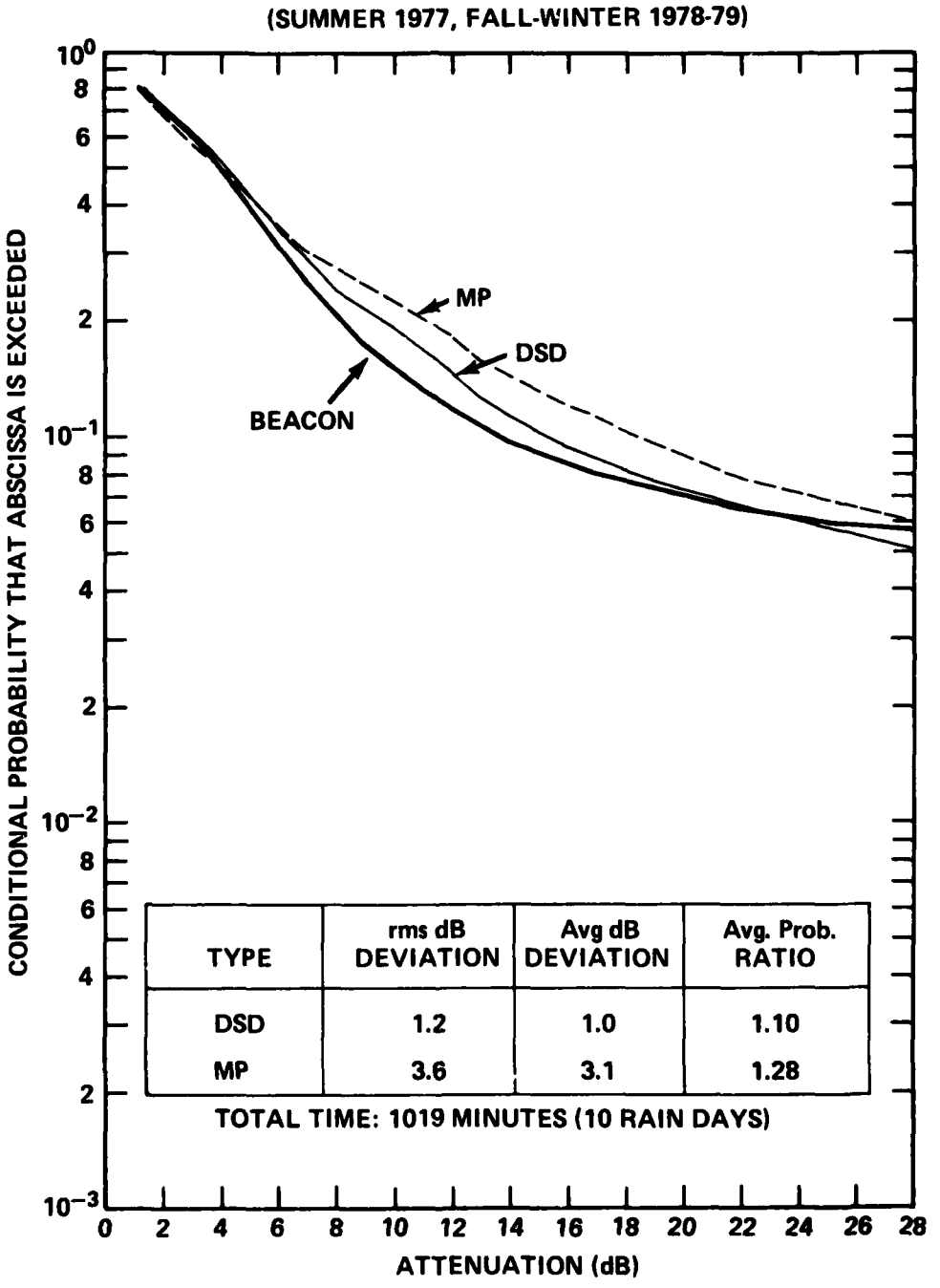

Figure 13. Comparison of overall conditional cumulative distributions combining summer and winter periods (ten rain days, 1019 minutes of simultaneous radar data).

Table 2

COMPARISON OF CUMULATIVE DISTRIBUTION CURVES

Period	Type	rms dB Deviation	Avg dB Deviation	Avg Prob Ratio	No of Minutes
1977 (summer)	DSD MP	1.2 5.6	1.0 5.0	1.09 1.37	304
1978-79 (fall-winter)	DSD MP	0.9 1.1	0.7 0.8	1.10 1.11	715
Overall	DSD MP	1.2 3.6	1.0 3.1	1.10 1.28	1019

melting regions. As illustrations, the reflectivity-height profiles for specific times during days 024, 065, and 094 are shown plotted in Figures 14, 15, and 16. The ordinate represents the height as measured along the earth-satellite path and the abscissa, the reflectivity factor in dBZ (10 Log_{10} Z). The indicated zero degree isotherm heights were obtained from radiosonde data and represent the average of heights measured at 0700 and 1900 EST. The enhanced reflectivity is a result of scattering from high concentrations of melting ice. Below the melting zone region, the ice changes completely into rain, the fall velocity increases and the concentration reduces resulting in reduced scattering. For cases showing a prominence of reflectivity about the zero degree isotherm, best results were, in general, obtained when the summation given by Eq. (3.1) was taken up to the base of the "nose" as depicted in the profiles of Figures 14, 15, and 16.

Evidence of a melting zone appears as a "bright band" on an RHI. A photograph of such an RHI is shown in Figure 17 which is grey scale coded in the sequence of black, grey, white, black, grey, white, where external black represents signals less than -90 dBm at the radar receiver mixer input and each grey scale change in sequence corresponds to a 10 dB enhancement interval. Hence, the black stratiform band above the 0^{o}C isotherm represents a power input to the mixer ranging between -60 to -70 dBm.

We show plotted in Figure 18 two radar estimated cases for day 024; one in which the summation is taken up to the base of the "nose" in Figure 14 and the other in which the summation is taken throughout the earth-satellite path. The profile in Figure 14 is taken at the time corresponding to location "a" in Figure 18. We note substantially improved agreement for the former case thus demonstrating the importance of examining Z-h profiles and RHI's of the type given in Figures 14 and 17, respectively, for improving radar derived attenuation techniques.

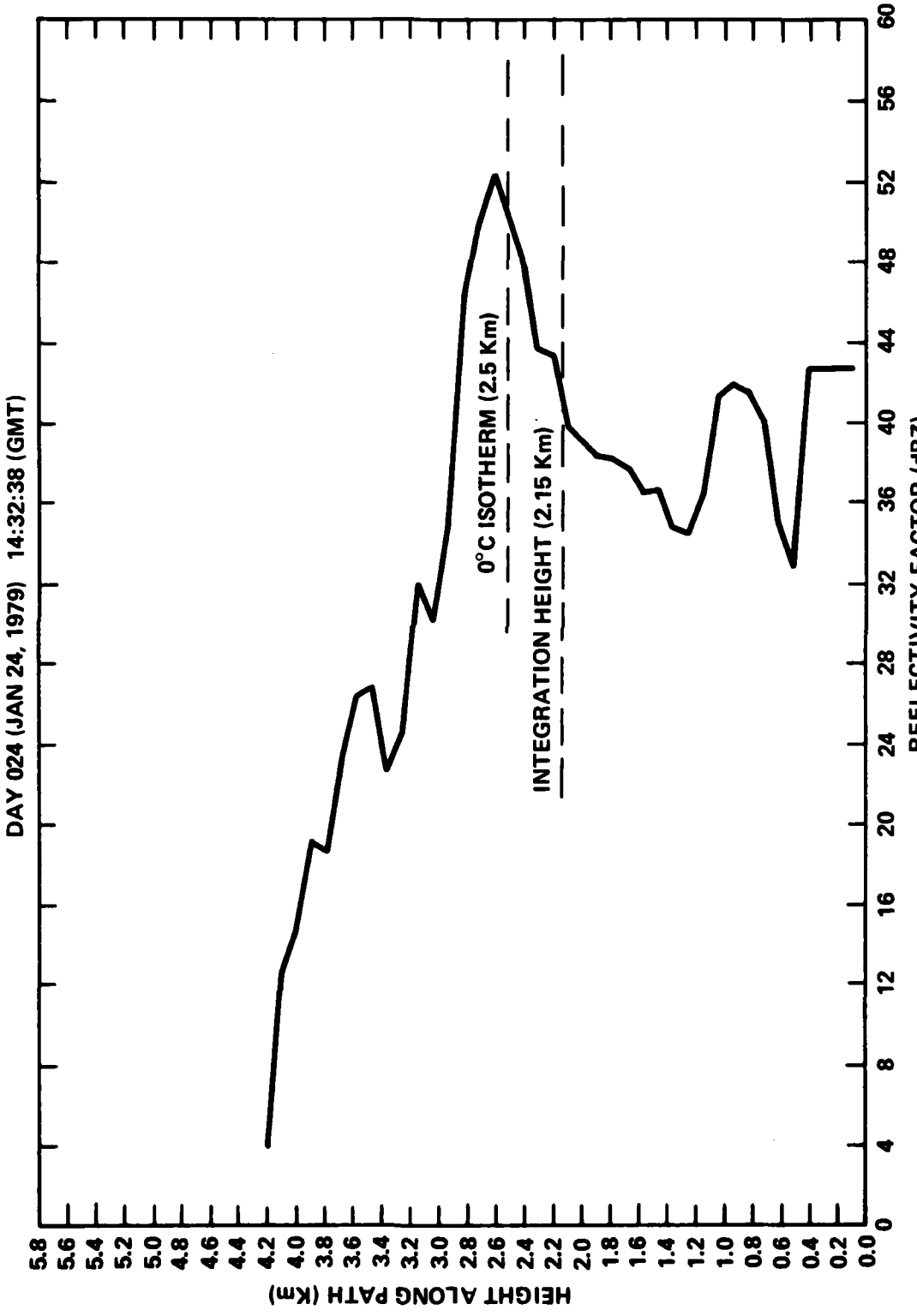

Figure 14. Reflectivity-height profile along earth satellite paths for January 24, 1979; 14:32:38 GMT, depicting melting layer about the 0°C isotherm height.

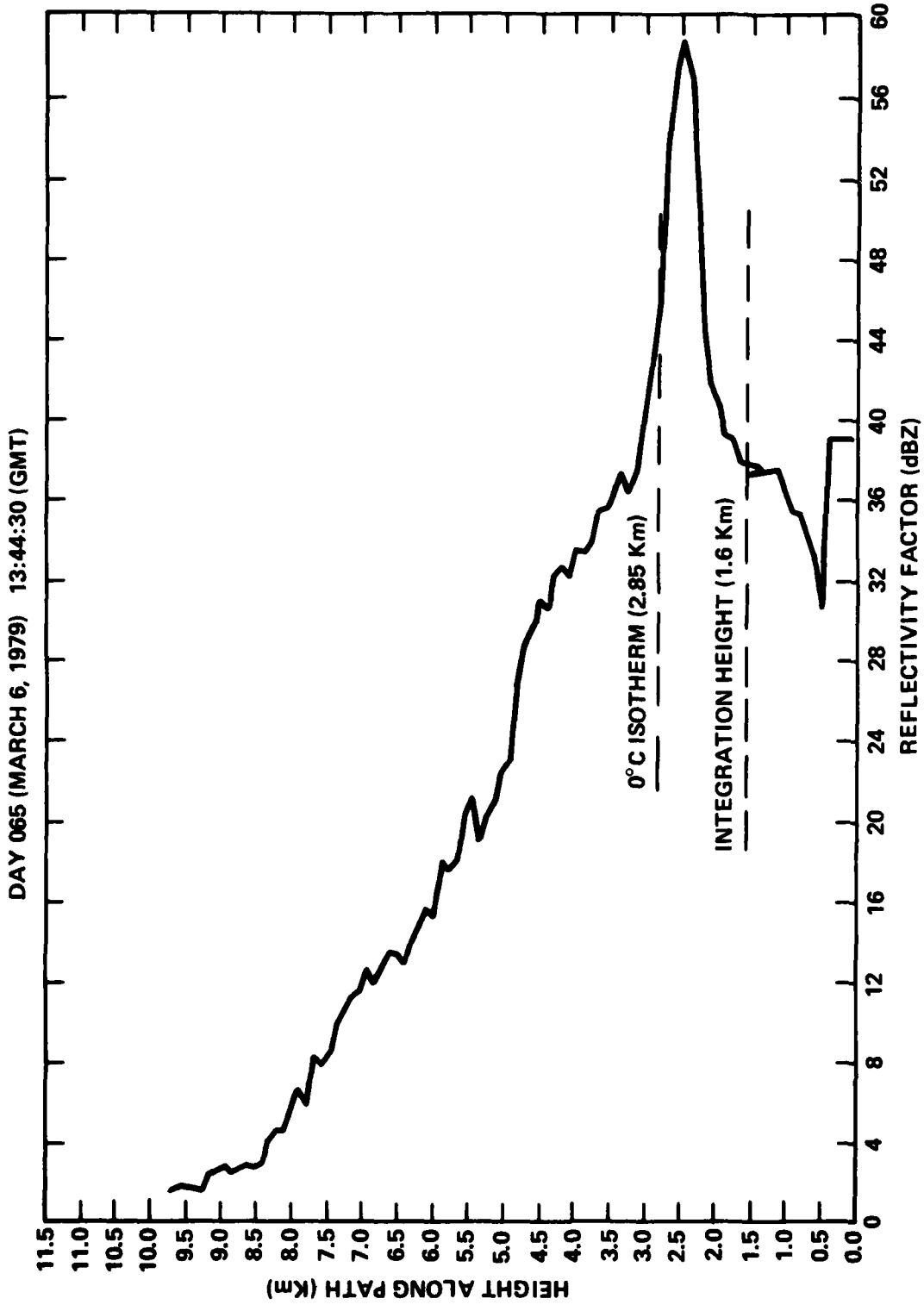

Figure 15. Reflectivity-height profile along earth-satellite path for March 6, 1979; 13:44:30 GMT, depicting melting layer about the 0°C isotherm height.

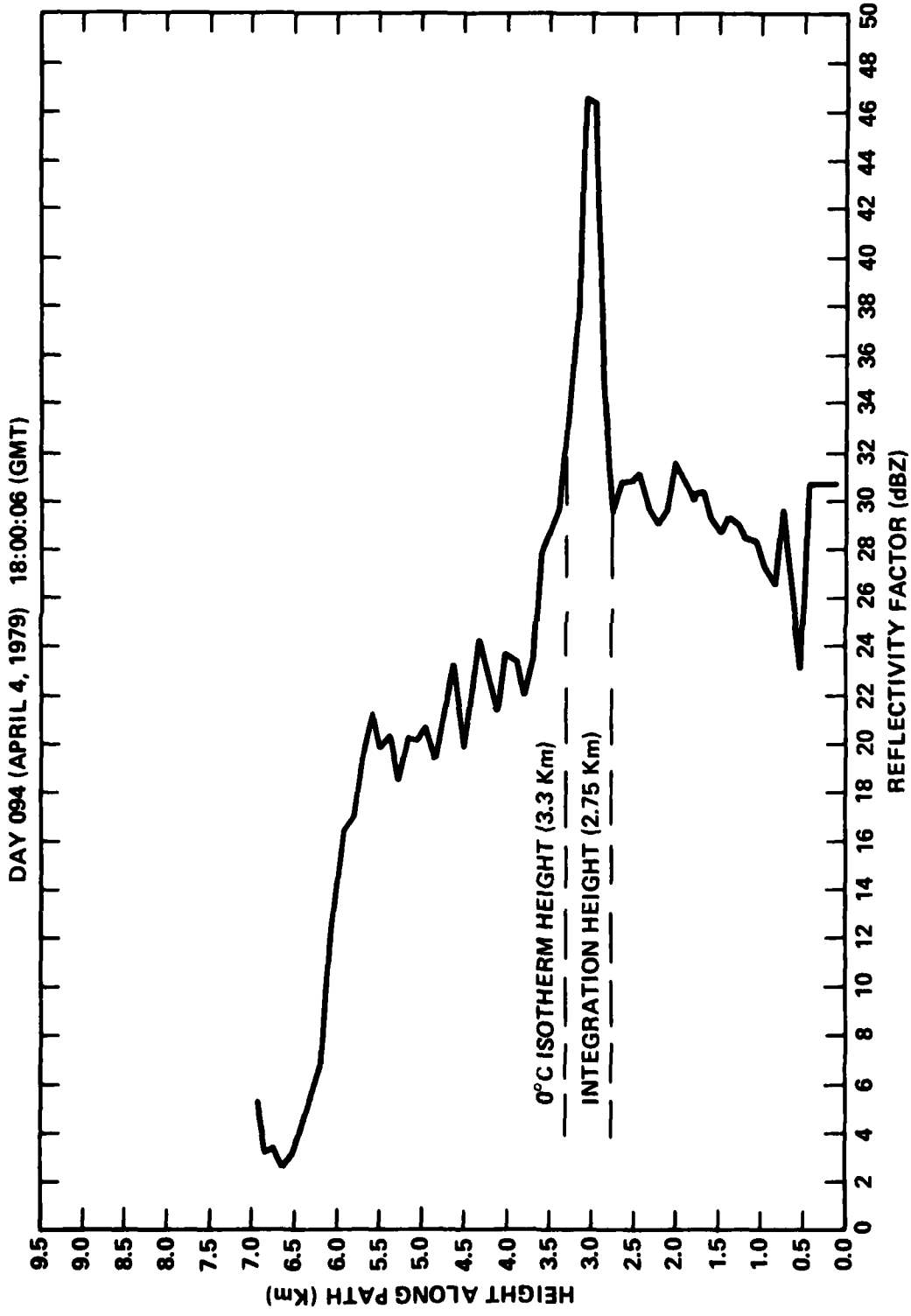

Figure 16. Reflectivity-height profile along earth-satellite path for April 4, 1979; 18:00:06 GMT, depicting melting layer about the 0°C isotherm height.

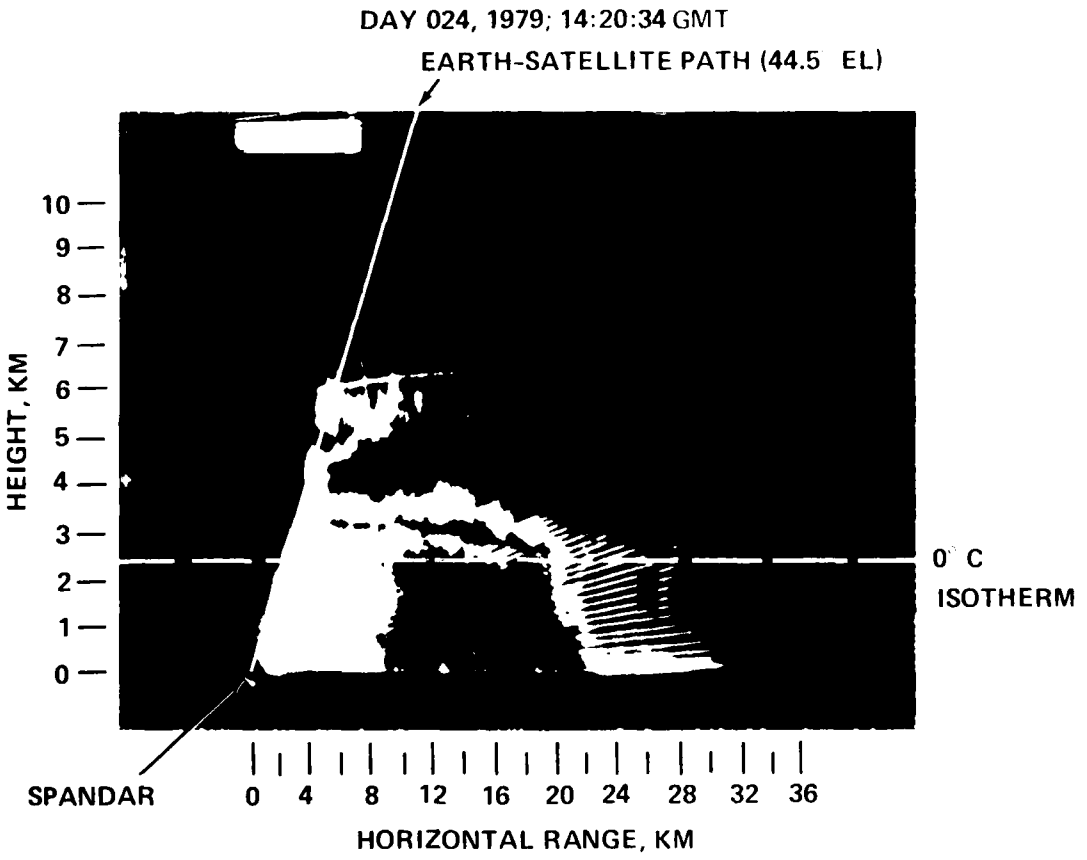

Figure 17. Coded photograph of RHI (Range Height Indicator) for January 24, 1979; 09:24:34 EST depicting stratiform and bright band. Grey scale code is in sequence black, grey, white, black, grey, white, where the first grey represents power levels between -80 and -90 dBm at the mixer input and each succeeding scale is within a 10 dB increasing power interval; external black representing power levels $\leq$ -90 dBm.

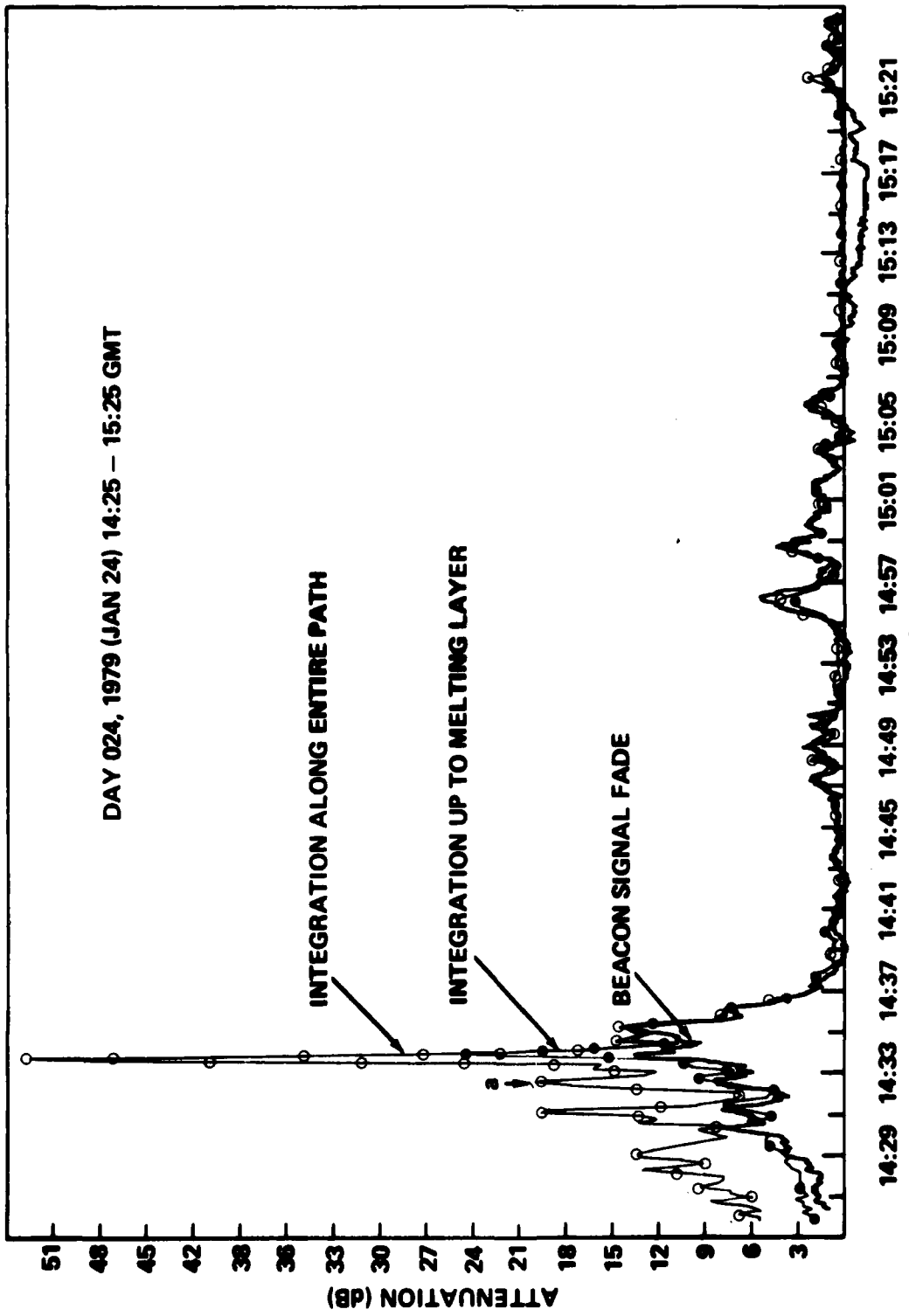

Figure 18. Influence of ice above the bright band on radar derived fade. Comparison shows radar derived fades where the path integration is taken both up and through melting layer. Also shown are the beacon measured fades (January 24, 1979; 1425 to 1525 GMT).

8.0 SUMMARY AND CONCLUSIONS

In Table 3 we summarize the previous comparisons using the generic descriptors excellent, good, fair, and poor. We conclude from this table which is based on approximately 17 hours of simultaneous radar, disdrometer, and beacon data flanking five summer and five winter rain days, the following:

(1) Radar is a generally good estimator of fade events and an excellent estimator of cumulative conditional fade distributions.

(2) A measurement of drop size spectra is desirable for each rain period so that the proper k-Z relationship may be established.

(3) The use of the Marshall-Palmer (10) k-Z relationship may be a reasonable alternative for the Wallops Island region.

Table 3

SUMMARY OF PREVIOUS COMPARISONS

Comparison Of:	Summer 1977	Fall-Winter 1978-79
(1) Individual fade events for DSD-radar and beacon cases	Good	Good
(2) Individual fade events for MP-radar and beacon cases	Fair	Good
(3) Overall DSD and MP k-Z regression relationships	Good-Excellent	Good-Excellent
(4) DSD-radar and beacon cumulative fade distributions	Excellent $\sigma_{rms} = 1.2$ dB $(P_1/P_2)_{avg} = 1.09$	Excellent $\sigma_{rms} = 0.9$ dB $(P_1/P_2)_{avg} = 1.10$
(5) MP-radar and beacon cumulative fade distributions	Fair-Poor $\sigma_{rms} = 5.6$ dB $(P_1/P_2)_{avg} = 1.37$	Excellent $\sigma_{rms} = 1.1$ dB $(P_1/P_2)_{avg} = 1.11$

9.0 REFERENCES

1. Goldhirsh, J. "Prediction Methods for Rain Attenuation Statistics at Variable Path Angles and Carrier Frequencies Between 13 and 100 GHz", IEEE Trans. on Antennas and Propagation, Vol. AP-23, No. 6, pp 786-791, November 1975.

2. Goldhirsh, J., "Path Attenuation Statistics Influenced by Orientation of Rain Cells", IEEE Trans. on Antennas and Propagation, Vol. AP-24, No. 6, pp 792-799, 1976.

3. Hodge, D. B., "Path Diversity for Earth-Space Communication Links", Radio Science, Vol. 13, No. 3, pp 481-487, May-June 1978.

4. Goldhirsh, J., "Prediction of Slant Path Rain Attenuation Statistics at Various Locations", Radio Science, Vol. 12, No. 5, pp 741-747, September-October 1977.

5. Cox, D. C., "An Overview of the Bell Laboratories 19 and 28 GHz COMSTAR Beacon Propagation Experiments", The Bell System Technical Journal, Vol. 57, No. 5, pp 1231-1255, 1978.

6. Goldhirsh, J., "Prediction Methods for Rain Attenuation Using Radar and In Situ Measurements Tested Against the 28 GHz COMSTAR Beacon Signals", IEEE Trans. on Antennas and Propagation, Vol. AP-27, No. 3, pp 398-406, May 1979.

7. Goldhirsh, J., "Prediction of Attenuation of the 28 GHz COMSTAR Beacon Signal Using Radar and Measured Rain Drop Spectra", APL/JHU Technical Report S1R78U-009, February 1978.

8. Goldhirsh, J., "Attenuation of Propagation Through Rain for an Earth-Satellite Path Correlated with Predicted Values Using Radar", IEEE Trans. on Antennas and Propagation, Vol. AP-24, No. 6, pp 800-806, 1976.

9. Medhurst, R. G., "Rainfall Attenuation of Centimeter Waves: Comparison of Theory and Measurement", IEEE Trans. on Antennas and Propagation, Vol. AP-13, pp 550-564, 1965.

10. Marshall, J.S. and W. McK. Palmer, "The Distribution of Raindrops with Size", Journal of Meteorology, Vol. 5, pp 165-177, 1948.

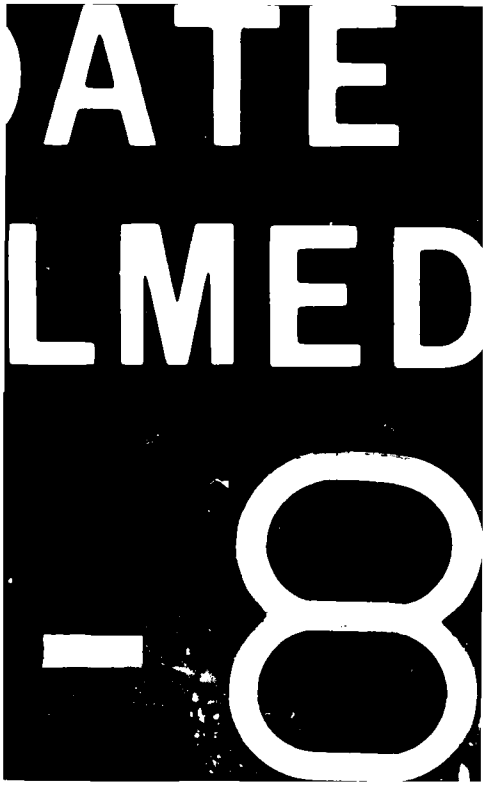
ATE
LMED
8